Decrease in Protein Solubility and Cataract Formation Caused by the Pro23 to Thr Mutation in Human γD-Crystallin † , ‡

ARTICLE *in* BIOCHEMISTRY · MARCH 2005

Impact Factor: 3.02 · DOI: 10.1021/bi0479611 · Source: PubMed

6 AUTHORS, INCLUDING:

Onofrio Annunziata
Texas Christian University
50 PUBLICATIONS **762** CITATIONS
SEE PROFILE

Jayanti Pande
University at Albany, The State University of …
58 PUBLICATIONS **1,929** CITATIONS
SEE PROFILE

Decrease in Protein Solubility and Cataract Formation Caused by the Pro23 to Thr Mutation in Human γD-Crystallin[†,‡]

Ajay Pande,[§] Onofrio Annunziata,[§,||] Neer Asherie,[§,⊥] Olutayo Ogun,[#] George B. Benedek,[§,#] and Jayanti Pande*[,#]

Department of Physics and Center for Materials Science and Engineering, and Materials Processing Center, Massachusetts Institute of Technology, Cambridge, Massachusetts 02139

Received September 21, 2004; Revised Manuscript Received November 23, 2004

ABSTRACT: The P23T mutation in the human γD-crystallin gene has in recent years been associated with a number of well known cataract phenotypes. To understand the molecular mechanism of lens opacity caused by this mutation, we expressed human γD-crystallin (HGD), the P23T mutant, and other related mutant proteins in *Escherichia coli* and compared the structures and thermodynamic properties of these proteins *in vitro*. The results show that the cataract-causing mutation P23T does not exhibit any significant structural change relative to the native protein. However, in marked contrast to the native protein, the mutant shows a dramatically lowered solubility. The reduced solubility results from the association of the P23T mutant to form a new condensed phase that contains clusters of the mutant protein. The monomer-cluster equilibrium is represented by a solubility curve in the phase diagram. When the solubility limit is exceeded, the mutant protein forms the condensed phase after a nucleation time of 10−20 min. We found that the solubility of the P23T mutant exhibits an inverse dependence on temperature, i.e., the protein clusters are increasingly soluble as the temperature of the solution decreases. The solubility of P23T can be substantially altered by the introduction of specific mutations at or in the immediate vicinity of residue 23. We examined the mutants P23S, P23V, P23TInsP24, and P23TN24K and found that the latter two mutations can restore the solubility of the P23T mutant. These findings may help develop a strategy for the rational design of small molecule inhibitors of this type of condensed phase.

The γ-crystallin genes that are most abundantly expressed in the human lens are CRGC, CRGD, and CRGS (*1*). While mutations linked to childhood cataracts have been found in all three genes, those affecting CRGD seem to be more numerous (*2*, *3*). It is now well recognized that cataracts associated with single-point mutations in any of these genes are in fact phenotypically heterogeneous. This is clearly illustrated by several recent reports in which the proline 23 to threonine (P23T)[1] mutation in CRGD has been found to be associated with several different cataract phenotypes, e.g., the corraliform cataract (*4*), the cerulean cataract (*5*), and the fasciculiform cataract (*6*). These reports also reveal how geographically widespread the P23T mutation is, because it appears in diverse population groups: India (*3*), the United States (*4*), Morocco (*5*), China (*6*), and Australia (*7*). Although there is abundant genetic data associating the P23T mutation in CRGD with the cataract, there is no clear understanding of the mechanism by which this mutation leads to lens opacity.

In previous reports, we showed that *in vitro* studies using recombinant human γD-crystallin (HGD) and its mutant proteins (*8*, *9*) can provide insights into the mechanism by which a genetic mutation leads to protein condensation and increased light scattering, which is responsible for the lens opacity observed *in vivo*. For example, in the juvenile cataract reported by Stephan et al. (*10*), which is associated with the R14C mutation in CRGD, we showed that, when Arg14 is replaced by Cys in HGD, Cys14 is so reactive that disulfide cross-linked aggregates of the mutant protein are rapidly generated. Furthermore, we showed that, while the mutant protein (R14C) remains monomeric when freshly produced, within minutes it forms large, disulfide cross-linked aggregates that eventually precipitate out of solution. Our results explained, in part, why children with the R14C mutation are born with clear lenses but over time develop the observed opacity (*8*).

[†] This work was supported by the National Institutes of Health Grants EY05127 (to G.B.B.) and EY10535 (to J.P.).

[‡] A preliminary account of this work entitled "Mechanism of opacity for an autosomal dominant form of congenital cataract" was presented at the 17th Symposium of the Protein Society, July 26−30, Boston, MA (2003).

* To whom correspondence should be addressed. Telephone: (617) 253-6804. Fax: (617) 225-2585. E-mail: jpande@mit.edu.

[§] Materials Processing Center.

[||] Present address: Department of Chemistry, Texas Christian University, Box 298860, Fort Worth, TX 76129.

[⊥] Present address: Department of Physics and Department of Biology, 2495 Amsterdam Avenue, Yeshiva University, New York, NY 10033-3312.

[#] Department of Physics and Center for Materials Science and Engineering.

[1] Abbreviations: HGD, recombinant human γD-crystallin protein; P23T, P23S, P23V, single mutants of HGD where proline is replaced by threonine, serine, and valine, respectively; P23TInsP24 and P23TN24K, single mutants of P23T in which proline is inserted in position 24 or glutamine 24 is replaced with a lysine, respectively; CRGX, member X of the γ-crystallin gene family (where X is A, B, C, D, E, or F); HbS, hemoglobin S; FTIR, Fourier transformed infrared; DTT, dithiothreitol; TEM, transmission electron microscopy; QLS, quasielastic light-scattering spectroscopy; CD, circular dichroism; LLPS, liquid−liquid phase separation.

10.1021/bi0479611 CCC: $30.25
Published on Web 02/01/2005

Table 1: List of Mutants and Corresponding Mutations Used in This Paper[a]

	20	23	26
human γD (HGD)	...Ser Asp His	Pro	Asn Leu Gln...
single mutants of HGD			
P23T	...Ser Asp His	Thr	Asn Leu Gln...
P23S	...Ser Asp His	Ser	Asn Leu Gln...
P23V	...Ser Asp His	Val	Asn Leu Gln...
single mutants of P23T			
P23TInsP24	...Ser Asp His	Thr Pro	Asn Leu...
P23TN24K	...Ser Asp His	Thr Lys	Leu Gln...

[a] Only partial sequences are displayed as indicated by the residue numbers.

In the cataracts associated with the R58H and R36S mutations in HGD, we showed that it was not protein aggregation but rather the ready crystallization of the mutant proteins that was responsible for the light scattering and opacity (*9*). Kmoch et al. (*11*) had already found that the cataract in a young patient was caused by light scattering due to the presence of crystalline material, which they showed to be the mutant protein, R36S. We subsequently showed using recombinant proteins *in vitro* that the R36S mutant rapidly crystallized at an unusually low concentration and that the solubility of the mutant protein was an order of magnitude lower than that of the native protein (*9*). In addition, we suggested that the mechanism of opacity for the R58H mutation in CRGD reported by Heon et al. (*12*) was also due to the ready crystallization of the R58H mutant protein, and our suggestion was subsequently confirmed by Heon and Munier (*13*).

A key element of our findings was that the cataractogenic changes caused by each of these mutant proteins occur without a significant change in the structure or stability of the protein. Thus, our studies with recombinant proteins have not only provided a molecular understanding of the disease but also demonstrated that a cataract-producing mutation does not need to be accompanied by a marked change in protein conformation or stability.

These studies provided the motivation for the work presented in this paper. Here, we show that the P23T mutant of HGD forms reversible aggregates (or clusters)[2] even at low protein concentrations. These clusters constitute the condensed phase, which is in equilibrium with protein monomers. The concentration of the monomers in solution is defined as the solubility at that temperature. The aggregate is the condensed phase, which is responsible for the light scattering and opacity resulting from this mutation. Again, as in the previous cases, we show that this form of protein condensation occurs without a significant change in the protein structure or stability. To better understand the mechanism of such aggregation and the structural implications of the replacement of Pro23, we have also expressed and examined several other mutants with different residues at and near the mutation site (Table 1). Our findings and conclusions are presented below.

[2] Throughout this paper, we have used the words "cluster" and "aggregate" interchangeably to indicate the new condensed phase. The word "aggregate" encompasses the smaller protein clusters that grow to form the larger condensates.

MATERIALS AND METHODS

Cloning, Expression, and Isolation of Proteins. Recombinant HGD was prepared by the amplification of the coding sequence from a human fetal lens cDNA library as detailed elsewhere (*8*). Overexpression of the recombinant proteins as well as their isolation and purification were all done according to the procedures described earlier (*8*). The forward and reverse primers used to make the mutant proteins were as follows.

Mutants of HGD

The P23T mutant

Forward: 5′-GCA GCA GCG ACC ACA CCA ACC TGC AGC CC-3′, *Reverse*: 5′-GGG CTG CAG GTT GGT GTG GTC GCT GCT GC-3′

The P23S mutant

Forward: 5′-GCA GCA GCG ACC ACT CCA ACC TGC AGC CCT AC-3′, *Reverse*: 5′-GTA GGG CTG CAG GTT GGA GTG GTC GCT GCT GC-3′

The P23V mutant

Forward: 5′-GCA GCA GCG ACC ACG TCA ACC TGC AGC CCT AC-3′, *Reverse*: 5′-GTA GG CTG CAG GTT GAC GTG GTC GCT GCT GC-3′

Mutants of P23T

The P23TInsP24 mutant

Forward: 5′-GCA GCA GCG ACC ACA CCC CCA ACC TGC AGC CC-3′, *Reverse*: 5′-GGG CTG CAG GTT GGG GGT GTG GTC GCT GCT GC-3′

The P23TN24K mutant

Forward: 5′-GCA GCA GCG ACC ACA CCA AGC TGC AGC CCT AC-3′, *Reverse*: 5′-GTA GGG CTG CAG CTT GGT GTG GTC GCT GCT GC-3′

All primers were synthesized by MWG Biotech Inc. (High Point, NC). Mutagenesis was performed with the QuikChange site-directed mutagenesis kit from Stratagene, and the plasmid DNA obtained after mutagenesis was sequenced with the T7 promoter primer and found to contain the desired mutation and no other sequence changes. The mutant and wild-type proteins were expressed in *E. coli* and purified as described earlier (*8*). In all cases, the crystallins were obtained from the soluble fraction. Every batch of purified crystallins was analyzed using electrospray ionization mass spectrometry (Biopolymers Laboratory at the Center for Cancer Research at the Massachusetts Institute of Technology). The average masses of six different batches of the proteins were as follows: HGD, 20 608 ± 1; P23T, 20 613 ± 1; P23S, 20 595 ±1; P23V, 20 608 ± 1; P23TInsP24, 20 710 ± 1; P23TN24K, 20 627 ± 1. The concentration of HGD was determined by using an extinction coefficient of 41.4 mM^{-1} cm^{-1} at 280 nm (*14*). This value was also used for the mutant proteins.

Electrospray Ionization Mass Spectrometry. Mass spectrometry was performed at the Biopolymers Laboratory as stated above. The molecular mass listed above for HGD is consistent with previously published work for the native protein to within 3 mass units (*8*, *9*). Masses listed for the

mutant proteins are consistent with the expected values derived from the appropriate amino acid replacements in HGD.

Solubility Studies. Solubility curves were obtained as follows. Aggregates of each of the mutant proteins were formed in one of two ways: (1) at a fixed protein concentration (C) as a function of increasing temperature (T) or (2) as a function of increasing C at a fixed T. After protein clusters formed under either condition, the suspension was allowed to settle, the supernatant was removed, and the sediment was dispersed in fresh buffer and gently stirred at a constant temperature. After some time, the clusters were found to dissolve partially. This new suspension was again allowed to settle, and the concentration of the protein monomers in the supernatant was sampled over a period of time, typically for 24−48 h until it reached a constant value. The system was considered to be at equilibrium when the protein concentration in the supernatant reached a constant value. Equilibrium was typically attained within 48 h. The equilibrium value of the protein concentration is taken as the solubility at that temperature and constitutes one point on the solubility curve. All solutions contained 20 mM dithiothreitol (DTT) to minimize oxidation of protein thiols. The contribution of DTT to the total absorbance was determined from SE-HPLC runs on a Superdex-200HR column (Pharmacia), using elution conditions described earlier (*15*).

The solubility curves for each of the mutants were obtained by plotting the equilibrium protein concentration corresponding to a given temperature for a series of temperatures in the range from −5 to 40 °C. The first measurements were performed at higher temperatures where the protein solubility was low. The temperature was then lowered, and the samples were equilibrated at the lower temperature so that more of the protein aggregates could dissolve and a new equilibrium value of protein solubility could be measured. Each solubility curve was measured for at least two different batches of samples.

Turbidity Measurements. The turbidity for a given protein solution was determined as follows. The solution contained in a test tube (inner diameter of 4 mm) was placed in a homemade cell connected to a circulating water bath. The actual temperature of the sample was measured (with a precision of 0.1 °C) by placing a thermocouple close to the test tube containing the sample. A 4 mW He−Ne laser was focused on the sample, and the transmitted light intensity was received by a photodiode. The transmitted light intensity, temperature of the sample, and the temperature setting of the water bath were all recorded.

The turbidity, τ, used to monitor clouding as a function of time, was calculated from $\tau = (1/L)\ln[I(0)/I(t)]$, where $I(0)$ is the initial value of the transmitted intensity, $I(t)$ is the transmitted intensity at time t, and L (=0.4 cm) is the inner diameter of the test tube. Most of the studies were conducted at 37 °C. To ensure that the initial samples were free from aggregates, they were prepared at 4 °C with the protein concentration below 5 mg/mL (i.e., below the solubility limit at 4 °C).

Circular Dichroism (CD) Spectra. CD spectra were obtained with an Aviv Associates (Lakewood, NJ) model 202 spectrometer as described previously (*8*). Protein concentrations of 0.5−1.0 mg/mL in 100 mM phosphate buffer (pH 7) were used for the near-UV CD spectra, and 0.1 mg/mL in 5−10 mM phosphate buffer were used for the far-UV CD spectra. CD spectra in the far-UV region were normalized with respect to the concentration of peptide bonds, whereas those in the near-UV region were normalized with respect to the protein concentration.

Fourier Transformed Infrared (FTIR) Spectroscopy. A total of 50 μL of a solution of HGD in water (concentration of ∼4−5 mg/mL) was spread on a CaF_2 plate and dried by blowing a uniform jet of argon gas. A suspension of the P23T mutant was centrifuged, and the pellet was washed once with water and resuspended. The slurry was spread on a CaF_2 plate and dried with argon gas. FTIR spectra were recorded on a Nicolet MAGNA860 spectrometer with an MCT detector. The spectra are the average of 1000 scans with a spectral resolution of 4 cm^{-1}.

Raman Spectroscopy. Raman spectra were measured using a Hololab 5000R modular research Raman spectrometer with a microprobe (Kaiser Optical Systems, Inc., Ann Arbor, MI) built around a DMLP optical microscope, as described earlier (*16*). Spectra were taken with a laser excitation at 514.5 nm from an argon ion laser (Coherent model Renova 306C, 6 W). The Raman spectrum of HGD was measured in a concentrated (≈2−3 mM) solution in water. To measure the Raman spectrum of the P23T mutant, we made a film of the protein because concentrated protein solutions could not be prepared as a result of the low solubility of P23T. The Raman spectra of the film of P23T deposited on a CaF_2 substrate (for FTIR measurements) were obtained also using an argon ion laser excitation at 514.5 nm. A 50× objective was used in the microscope, and a small uniform region in the film was sampled. Laser power at the sample was 14 mW. Raman spectra were dispersed at a spectral resolution of 5 cm^{-1} and detected using a thermoelectrically cooled CCD detector at −40 °C (1024 × 256 front illuminated camera from Andor Technology).

Quasielastic Light-Scattering Spectroscopy (QLS). QLS experiments were performed using a homemade light-scattering apparatus using a PD2000DLS^{PLUS} correlator (256 channels; Precision Detectors, Bellingham, MA) and a coherent He−Ne laser (35 mW, 632.8 nm; Coherent Radiation, Santa Clara, CA). The scattering angle was 90°. All protein samples were filtered using a 0.02 μm Millipore filter and placed in a test tube. The temperature of the sample holder was controlled using a water bath. The actual temperature of the sample was measured (with a precision of 0.1 °C) by placing a thermocouple close to the test tube containing the sample. The measured correlation functions were analyzed by the Precision Deconvolve 4.4 software provided by Precision Detectors. This software, which employs a constrained regularization method, is used to determine the scattered intensity versus diffusion coefficient.

Transmission Electron Microscopy (TEM). TEM images were collected from Formvar and carbon-coated nickel grids prepared by adding 10−20 μL of the protein sample at a concentration of 1 mg/mL. The grids were then washed with water and negatively stained with 10 mL of uranyl acetate. Images were collected on a Phillips EM410 transmission electron microscope at 80 kV excitation voltages.

Liquid−Liquid Phase Separation (LLPS). LLPS was exhibited only by the P23V, P23TInsP24, and P23TN24K mutants. Coexistence curves were obtained by the cloud point

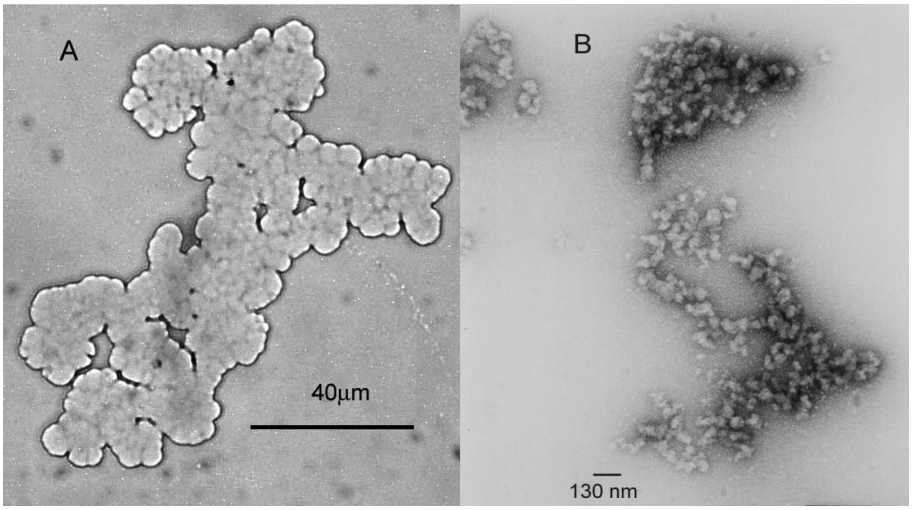

FIGURE 1: Aggregates of the P23T mutant as viewed under the Nikon Optiphot-pol light microscope (A) and the Philips EM410 transmission electron microscope (B). Protein concentration of 1 mg/mL in 0.1 M sodium phosphate buffer at pH 7. TEM picture taken by Nicki Watson at the W. M. Keck Foundation Biological Imaging Facility at the Whitehead Institute at M.I.T.

and temperature quench methods using procedures well-established in this laboratory and published earlier (*17*).

RESULTS AND DISCUSSION

Our results show that the P23T mutant of HGD cannot be concentrated above 1−2 mg/mL at ambient temperatures (22−24 °C). Above this concentration, the protein condenses to form aggregates or clusters that grow to a critical size and sediment. In contrast, HGD, just like the other highly homologous γ-crystallins (*17*), can be concentrated to over 400 mg/mL without any protein precipitation whatsoever. Thus, the dramatic lowering in the solubility of the P23T mutant relative to the native protein is directly responsible for the light scattering and opacity caused by the Pro23 to Thr substitution.

Cluster Formation. We examined cluster formation using QLS. In all of our QLS measurements, we found that initially the solution of the P23T mutant was monomeric and transparent for at least 10−20 min, with a time-independent and monomodal distribution of the scattering intensity. The value of the hydrodynamic radius and mean diffusion coefficient determined within this time period ($R_h \approx 24$ Å) was consistent with those reported previously for several monomeric γ-crystallins (*18*). After an induction time of 10−20 min, we were unable to make further QLS measurements because large clusters are suddenly formed in solution. The presence of an induction time indicates that the aggregation of P23T is driven by a nucleation event.

Morphology of the Aggregates. The diffuse, unstructured aggregates observed in solutions of P23T were examined under a light microscope (Figure 1A) as well as under a transmission electron microscope (Figure 1B). TEM studies of the condensed phase show amorphous solid clumps about 40−50 nm in size (Figure 1B), while light microscopy shows larger deposits (about 2−5 μm). Clusters in this range of sizes are present together in the condensed phase. A similar range of sizes in the "dense globular deposits" was observed by Shentu et al. (*6*) in the TEM pictures of lens tissue obtained from the P23T cataract-affected individuals. Although a direct comparison cannot be made, it is significant that the distribution of sizes observed by us *in vitro* is within the same range as that of the "dense globular deposits" reported by these authors *in vivo*. We note that neither light microscopy nor TEM showed any evidence of periodic structures such as crystals or fibers in our studies.

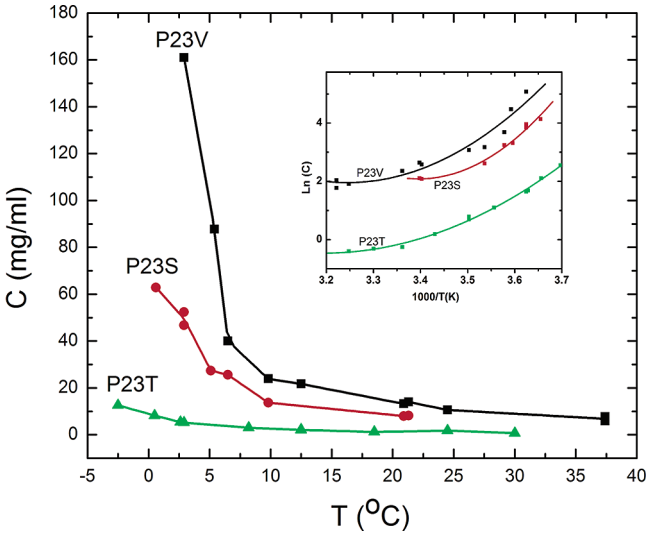

FIGURE 2: Solubility of the mutants of human γD-crystallin at various temperatures. Measured here is the concentration of the soluble protein remaining in the supernatant after the equilibrium is established with the insoluble phase containing the protein aggregates shown in Figure 1. (Inset) van't Hoff plots of the same data showing nonlinearity. Lines drawn through these data are merely visual guides.

Temperature Dependence of the Solubility of P23T. At any given temperature, the aggregates of P23T can be dissolved to reach equilibrium with the protein monomer in solution such that there is a well-defined solubility at that temperature. From Figure 2, which shows the solubility curve for the P23T mutant, it is apparent that the solubility of P23T (which represents protein monomer-aggregate equilibrium) *decreases* as the temperature increases. This is in marked contrast to the case of the protein monomer-crystal equilibrium in which we showed that the solubility *increases* with increasing temperature (*9*, *19*, *20*). The inverted solubility curve for P23T is similar to that observed for hemoglobin S (HbS) (*21*), small hydrocarbons (*22*, *23*), and micelle

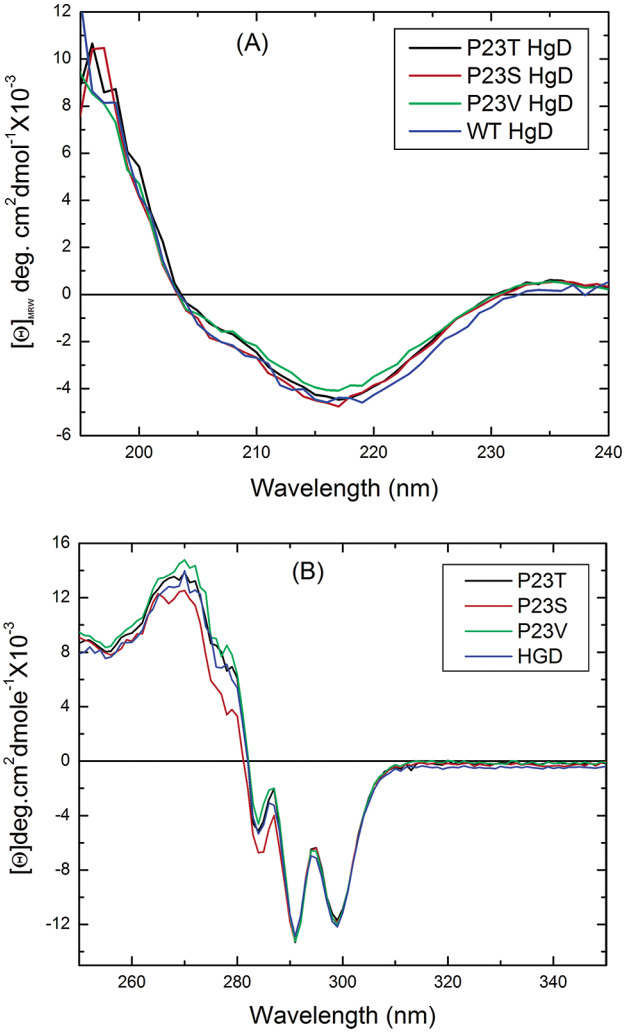

FIGURE 3: (A) Far-UV and (B) near-UV CD spectra of HGD and its mutants. Protein concentrations of 0.1 mg/mL in 5 mM sodium phosphate buffer at pH 7 in the far-UV region and 0.5-1.0 mg/mL in 100 mM sodium phosphate buffer in the near-UV region. Other details are mentioned in the Materials and Methods.

formation at concentrations approaching the critical micelle concentration (*24*). In all of these systems, the inverted temperature dependence of solubility has been associated with hydrophobic intermolecular interactions.

Structure and Stability Studies. To evaluate if this mutation was accompanied by a structural and conformational change in the protein, we also compared the CD spectra of HGD and P23T in the far- and near-UV regions. The CD spectra in the far-UV region, which monitors the secondary structure of proteins, are shown in Figure 3A, and those in the near-UV region, which monitors the tertiary structure of proteins, are shown in Figure 3B. These spectra are nearly identical for both HGD and P23T, suggesting that this cataract-causing mutation occurs without a significant conformational change, as in the other cases that we examined earlier (*8*, *9*). In addition, both proteins are very similar in their thermal stabilities, as measured by the loss of ellipticity in the near-UV region, as a function of temperature. We found that both proteins unfold eventually around 80 °C and precipitate at this temperature (data not shown). These results clearly suggest that, at least at the monomer level, HGD and P23T are nearly identical in their structure and stability.

However, CD only probes the structure of the protein in solution. Since the mutant protein undergoes aggregation and precipitation, we wondered whether a structural change could have occurred in the insoluble precipitate of P23T. To address this question, we examined the secondary structure of the protein in the insoluble form using FTIR and Raman spectroscopies.

Vibrational Spectra. Raman and FTIR spectroscopies have been widely used to determine the overall structure of insoluble proteins such as those associated with neurological diseases (*25*, *26*). Ideally, for P23T, we would have preferred to compare the structure of the mutant protein in the insoluble precipitate with that in the solution state. This was not possible because the solubility of P23T is very low at ambient temperature (Figure 2) and both Raman and FTIR techniques require high protein concentrations (in the millimolar, ∼10−100 mg/mL, range). Thus, the low solubility of P23T precludes a direct comparison of the secondary structure of the mutant protein in the liquid and solid states. However, an indirect comparison is still possible in view of the fact that the secondary structure of P23T in the soluble form is very similar to that of HGD (Figure 3). We have therefore compared the Raman spectra of HGD in solution, as a reference, with that of the P23T precipitate.

In FTIR spectroscopy, a direct comparison of both proteins is possible if the spectra are obtained in dry, thin films of the protein. In this manner, the large contribution of solvent water to the amide-I absorption band of the protein is virtually eliminated (*26*). In fact, in an attempt to minimize errors in the evaluation of secondary structure, a recent study (*27*) concludes that the amide-III band in the IR spectrum of proteins (∼1200−1350 cm^{-1}) may be a more accurate indicator of protein secondary structure than the amide-I band. We therefore compared both the amide-I and amide-III bands for the two proteins.

The vibrational spectra (FTIR and Raman) of HGD and P23T are shown in Figure 4. The main section of Figure 4 shows that the FTIR spectra of both HGD and P23T have closely similar amide-I bands centered around 1639 cm^{-1} and amide-III bands centered around 1235 cm^{-1}, typical of β sheet proteins (*28*). While the amide-III bands for the two proteins are nearly identical, the slight difference in the amide-I band profile is likely to be due to the unequal retention of residual water in the two cases. From these data, we conclude that the film of the P23T mutant probably retains more water than that of HGD. This is consistent with our observation that films of the P23T aggregate−precipitate appeared opaque-white and adhered better to the CaF_2 substrate, while those made from HGD were semi-transparent and peeled off the substrate more readily.

The inset to Figure 4 shows that the main feature of the Raman spectrum, the amide-I band, is very similar for the two proteins and is centered around 1672 cm^{-1}, a frequency typical of predominantly antiparallel β-sheet-containing proteins (*29*, *30*). Thus, on the basis of the amide-I band in the Raman spectra and the amide-III band in the FTIR spectra, we conclude that the protein structure of P23T, even in the insoluble phase, is essentially the same as that of the native protein. It should be noted that there are other examples where little structural change is observed in the protein even when it forms an insoluble phase. It has been shown that QHF-lithostathine, a protein found in human brain

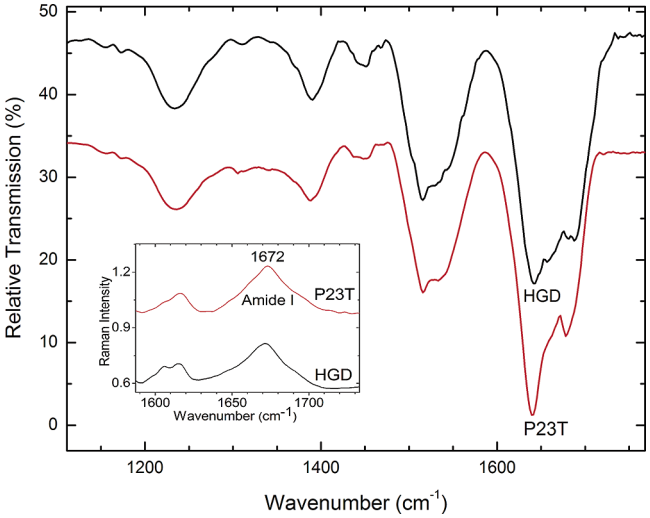

FIGURE 4: FTIR spectra of HGD and P23T in the amide-I to amide-III spectral regions. Spectra were obtained from protein films deposited on a CaF_2 substrate. HGD film was obtained by drying a solution of the protein under argon, while the P23T film was obtained by drying the aggregated protein pellet under argon. See the Materials and Methods for details. (Inset) Raman spectra of the proteins in the amide-I region. The HGD spectrum was measured in a 2−3 mM protein solution, while that of P23T was obtained from a film of the aggregated protein as described in the Materials and Methods under FTIR and Raman spectroscopy. For ease of comparison, the spectra of the two proteins are offset by a constant.

and pancreas, forms fibers that do not bind Congo red and thus do not show the birefringence typical of fibers that do bind Congo red. These fibers consist of the protein in its native conformation (*26*). Another example is a yeast prion protein Ure2p (*31*), where fibers are formed and the native protein structure within the fiber remains intact. A third, well-established example is the fiber formed from sickle-cell hemoglobin (*21*) in which the protein within the fibers also maintains the native conformation.

Thus, our results demonstrate that the lowered solubility of the P23T mutant shown in Figure 2, relative to the native protein, HGD, cannot be explained on the basis of a significant structural change in the protein and must arise predominantly from an increase in the net protein-protein attractive interactions.

Protein Mixtures. Since the P23T mutation is associated with an autosomal dominant form of the cataract, the lens fiber cells *in vivo* are likely to contain mixtures of P23T and HGD. Therefore, to understand how the aggregation of P23T is affected by the presence of HGD, we decided to examine mixtures of the two proteins *in vitro*. In particular, because HGD and P23T are structurally almost identical (as discussed above), we wondered about the possibility of mixed aggregate formation.

We examined the aggregation of P23T/HGD mixtures at 37 °C and several other temperatures and observed that, when the concentration of P23T is below the solubility limit at a given temperature (Figure 2), no aggregates are formed irrespective of the concentration of HGD in solution. This suggests that HGD does not participate in the formation of insoluble aggregates. However, when the concentration of P23T is above the solubility limit, the presence of HGD does affect the kinetics of aggregation. More specifically, for any given concentration of P23T above the solubility limit (Figure 2), the rate of aggregation, as monitored by turbidity measurements, decreases as the concentration of HGD is increased. This observation suggests that, above the solubility limit at a given temperature, HGD interferes with the attachment of P23T proteins to each other thereby retarding the rate of aggregation of P23T. One mechanism for this interference could be a reversible association between HGD and P23T. While the existence of the P23T clusters suggests the presence of multiple sticky sites or attractive patches on this mutant, our mixture experiments suggest that these sites can be screened by HGD.

Effect of Alternative Replacement of Pro23 on Protein Structure and Solubility. On the basis of structural considerations alone, one might expect that, when the relatively nonpolar Pro residue in HGD is replaced by a Thr with a strongly polar −OH side chain, the solubility of the resulting mutant, P23T, would actually increase. However, as our data show, the opposite behavior is observed and the mutant protein has a dramatically lowered solubility relative to HGD. To investigate this apparent paradox, we made a mutant of P23T in which we replaced the Thr residue with a structurally similar Ser to produce the P23S mutant. We then compared the structure and solubility of the P23S mutant with that of P23T and found that, in the overall structure measured by the CD spectra, both mutants are closely similar to that of the native protein (parts A and B of Figure 3). Furthermore, the P23S mutant also forms clusters very similar to those of the cataractogenic mutant, P23T. However, the solubility curve for P23S is shifted to higher protein concentrations at lower temperatures, implying that P23S is *significantly more soluble* than P23T (Figure 2). We then explored the effect of replacing the polar −OH group of Thr and Ser with a nonpolar $-CH_3$ group by replacing Pro23 with a Val. We found to our surprise that the P23V mutant, while it also forms clusters similar to those of P23T and P23S, is in fact *far more soluble than either* P23T or P23S (Figure 2). In fact, we found that the solubility of P23V approaches native-like values at lower temperatures. In addition, with the P23V mutant, we are able to observe LLPS, which is typically observed for HGD and other native γ-crystallins (*8*, *17*), whereas for the P23T and P23S mutants, LLPS could not be observed (Figure 5). Again, as in case of P23T and P23S, the shift in the solubility curve of P23V occurs without any change in the overall structure of the protein (parts A and B of Figure 3).

The results described above and shown in Figure 2 vividly demonstrate the very significant shifts in the solubility phase boundaries that can be brought about by point mutations at site 23 in HGD. To obtain a quantitative measure of these changes, we plotted the data shown in Figure 2 as a conventional log C versus $1/T$ (or van't Hoff) plot (inset of Figure 2) and found that the data are nonlinear in $1/T$. The nonlinearity of the van't Hoff plot indicates that the enthalpy and entropy changes are strongly temperature-dependent, as observed in the case of the solubility of HbS (*21*) and hydrocarbons in water (*24*). The temperature dependence of the enthalpic and entropic changes therefore precludes a simple thermodynamic analysis of the energetics of this type of cluster condensate. This behavior should be contrasted with the thermodynamic analysis of the monomer−crystal equilibria in which the van't Hoff plots are linear (*9*). Further insight into the inverted temperature dependence of the

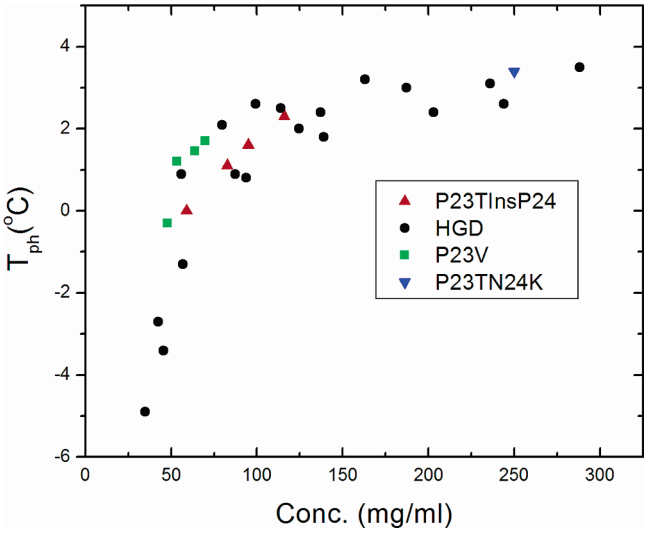

FIGURE 5: Coexistence curves for the LLPS of HGD and its various mutants. While only a few data points have been obtained for P23V and P23TInsP24, it is clear that these data lie on the same curve as that of HGD. Only one datum point was obtained for P23TN24K, to demonstrate its high, nativelike solubility. This point also essentially lies on the same curve as HGD.

Table 2: Primary Sequence Alignment for the Arbitrarily Chosen First 34 Residues of Human γD-Crystallin and Some of Its Homologues[a]

	1 23 34
CRGD human	GKITLYEDRGFQGRHYECSSDHPNLQPYLSRCNS
CRGD bovine	GKITFYEDRGFQGRHYECSSDHSNLQPYLGRCNS
CRGB bovine	GKITFYEDRGFQGHCYECSSDCPNLQPYFSRCNS
CRGB mouse	GKITFFEDRSFQGRCYECSSDCPNLQTYFSRCNS
CRGB rat	GKITFFEDRGFQGRCYECSSDCPNLQTYFSRCNS
CRGC human	GKITFYEDRAFQGRSYETTTDCPNLQPYFSRCNS
CRGC mouse	GKITFFEDRSFQGRCYECSSDCPNLQTYFSRCNS
CRGC rat	GKITFYEDRGFQGRCYECSSDCPNLQTYFSRCNS
CRGD mouse	GKITFYEDRGFQGRHYECSTDHSNLQPYFSHCNS
CRGD rat	GKITFYEDRGFQGRHYECSTDHSNLQPYFSRCNS

[a] As shown here, proline 23 in human γD-crystallin is replaced by a serine in some of these homologues. Identical residues in all proteins are shown in a gray background, and the rest are in a black background.

solubility of the mutants shown in Figure 2 may be obtained by calorimetrically measuring the change in heat capacity accompanying the aggregation process. These calorimetry studies are currently being pursued.

Primary Sequence Comparison with Homologous Proteins. To better understand our results in terms of the primary sequence of HGD, we compared the amino acid sequence of HGD with those of several members of this highly homologous family of crystallins. Table 2 shows that Pro23 is often replaced by Ser in the γ-crystallins from several different species. In each of these cases, there is no adverse effect on the structure or solubility. One such example is bovine γD-crystallin (BGD) with a Ser in position 23, which we have shown earlier to be identical to HGD in nearly all of its phase-transition properties (*8*, *17*). Therefore, it would appear that Ser and Pro have comparable intra- and inter-

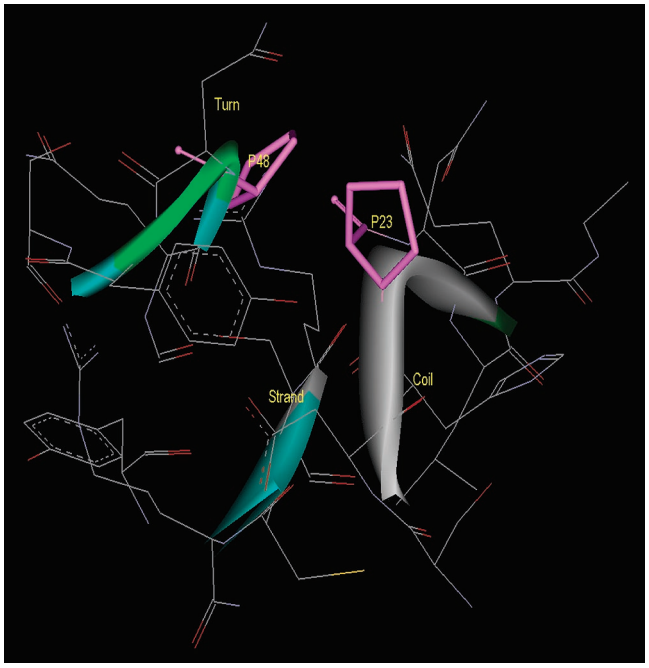

FIGURE 6: Section of the X-ray structure of HGD, which lies within an 8 Å sphere around residue P23. The two prolines, P23 and P48 are highlighted in pink. The protein loop (or coil) containing P23 is also shown as a white gray tube. Another loop (or turn) on the opposite side, shown as a green tube, contains P48. Together these turn and coil structures appear to cover a section of the β strand, shown in a sky-blue band underneath them. The picture was made using DS Viewer Pro from Accelrys.

molecular interactions in these proteins. However, as we have seen from the data in Figure 2, this is clearly not true for the P23S mutant of HGD, which has a dramatically lower solubility than HGD.

We should point out that this is not the only instance in which a single-point mutation affects the solution properties of one member of an orthologous family of proteins significantly while leaving the other members unaffected (*32*). Another example is the A53T mutation in α-synuclein, which is associated with Parkinson's disease in humans, but is found in several orthologues of α-synuclein in other species (*33*) without pathologic effects. These examples clearly demonstrate how a point mutation that has a profoundly deleterious effect on one member of a homologous family can leave the others functioning normally.

Effect of Point Mutations at Site 24. From the high-resolution X-ray crystal structure of HGD (*34*), we found that Pro23 is located in the middle of a long loop in the protein structure (Figure 6). Nandrot et al. (*5*) have modeled the structure of the P23T mutant and observed that no significant perturbation of protein structure occurs when Pro is replaced by Thr. Similarly, as stated in previous paragraphs and shown by the CD spectra in parts A and B of Figure 3, we have found that Pro can also be substituted by Ser or Val without any significant perturbation in the protein structure. However, no particular structural feature stands out that would explain the lower solubility of the P23T mutant.

Our results obtained with the single-point mutations discussed above suggested that it may be the absence of a proline residue, rather than the introduction of a threonine residue, that leads to the aggregation of P23T. To examine

this hypothesis, we made a mutant in which, in addition to the P23T mutation, we inserted a proline at position 24 (P23TinsP24, Table 1). Remarkably, we found that this new mutant *restores* the solubility of P23T to native-like values and exhibits LLPS similar to that of the native protein (see Figure 5). Furthermore, the P23TInsP24 mutant also shows a native-like protein structure (CD data not shown). These data highlight the importance of a Pro residue in the loop in preventing the formation of this type of condensate in HGD.

In view of the results reported above with the P23TInsP24 mutation, it was natural to consider if other mutations in P23T in the vicinity of position 23 could similarly protect the protein from condensation. There is indication in the literature that the introduction of a lysine residue at or near a possible protein-protein interface can inhibit aggregation and increase solubility (*35*−*37*). In a survey of the intermolecular contacts in protein crystal lattices, as well as of the intersubunit contacts in oligomeric proteins, it was observed that lysine is rarely found at protein-protein interfaces (*38*, *39*). In fact, it has been shown that the replacement of a surface lysine residue facilitates the crystallization of proteins, while the reverse, i.e., the introduction of a lysine residue, inhibits crystallization and aggregation (*40*, *41*). With these observations in mind, we made yet another mutant of P23T, with Asn24 replaced with a Lys (i.e., P23TN24K, Table 1), and found that the P23TN24K mutant also *does not* aggregate and *restores* the solubility of P23T to native-like values just like the P23TInsP24 mutant. Furthermore, this mutant also shows an overall structure identical to that of the native protein and exhibits native-like LLPS (Figure 5). We should mention that the data shown in Figure 5 for the P23V, P23TInsP24, and P23TN24K mutants simply illustrate that native-like LLPS behavior can be restored by specific mutations at or near site 24. These data are not intended to serve as detailed investigations of the coexistence curves of these proteins. Further studies with a larger set of mutants are ongoing and should ultimately provide a more comprehensive understanding of how solubility can be controlled in these proteins.

Role of Pro23 in Modulating Protein-Protein Interactions. We offer a structural interpretation for the importance of Pro23 in HGD and the consequences of its replacement in P23T. We speculate that the low solubility of P23T leading to aggregation is facilitated by the formation of a particularly attractive patch at or near the mutation site (*34*). The magnitude of this attraction can clearly be strongly modulated by the nature of the residues that are placed in the vicinity of the mutation site, as our data show. In the case of P23T, the replacement of Pro23 with Thr could generate a strongly attractive patch directly at the mutation site, which could then lead to the initial protein-protein association.

However, there may be another mechanism by which a strong, attractive surface is generated. Figure 6 shows that the loop containing Pro23 is located in close proximity to an edge β strand shown in cyan. The association or stacking of exposed β strands is a well-known phenomenon in many proteins (*35*). In native HGD, the edge strand (Figure 6) appears to be shielded by the loop containing Pro23 and the turn containing Pro48. Removing Pro23 may make this β strand accessible and promote strand-strand interaction and stacking to form the initial condensate.

Whatever may be the mechanism by which an attractive patch is generated, we recognize that a direct patch-patch interaction alone cannot form the nucleus that promotes cluster formation. Moreover, the inverse temperature dependence of solubility (see Figure 2 and the section entitled *Temperature Dependence of the Solubility of P23T*) shows that the overall energetics are governed by hydrophobic interactions and not hydrogen bonds that would form in strand-strand interaction. In earlier reports from this laboratory, we have shown that, in general, the γ-crystallins are characterized by weak attractive patches on the surface and net attractive interactions between the protein molecules (*42*, *43*). We speculate that, in the case of the P23T mutant, the strongly attractive patch at or near the mutation site may first interact with a different site on a neighboring molecule. This association increases the dwell time for other neighboring molecules to coalesce and begin the process of forming the initial nucleus. This nucleation step is analogous to that found in the condensation of HbS (*21*). Once the nucleus reaches a critical size, the formation of the macroscopic condensed phase becomes possible after an experimentally determined induction time for nucleation of about 10−20 min (see Materials and Methods). Overall, as shown by the solubility data, the condensation of P23T occurs by means of net hydrophobic interactions between the protein molecules.

CONCLUSIONS

Our results show that the P23T mutation in human γD-crystallin dramatically lowers the solubility of the protein.[3] The lowered solubility is due to the formation of a new "cluster" condensed phase, which is responsible for the light scattering and opacity. The solubility curve representing the protein cluster-monomer equilibrium is distinct from that of the protein crystal-monomer solubility curve (or liquidus line) reported in our earlier publications (*9*, *19*, *20*). Therefore, the cluster phase constitutes a new feature in the phase diagram of the γ-crystallins. Our work also suggests that the nature of the residue at location 23 appears to be important in maintaining the solubility of native HGD. We have shown that by replacing Pro23 with Ser or Val instead of Thr progressively increases the solubility of the protein such that it approaches that of native HGD.

The P23T mutation is yet another example of a mutation of human γD-crystallin that leads to cataract formation without altering the overall protein structure. This is consistent with our earlier suggestion that a cataractogenic condensed phase can occur without a significant change in protein structure or stability (*8*, *9*).

Finally, our results with the P23TInsP24 and P23TN24K suggest that the local protein environment around residue 23 can also be altered to effectively shift the solubility curve. We find that, by introducing specific residues at location 24 immediately adjacent to the mutation site, we can restore the solubility of the mutant to nativelike values. These results

[3] While this paper was under review, Evans et al. (*44*) published their results on the P23T and P23S mutants of human γD-crystallin and concluded, as we do here, that the cataract results from the lowered solubility of the P23T mutant protein. Besides this common conclusion, our study is distinct from the one published by these authors.

therefore suggest a possible strategy for the rational design of small molecule inhibitors of this type of condensed phase.

ACKNOWLEDGMENT

We thank Dr. Nicolette Lubsen for providing the original human CRGD clone for all of our work and Dr. Aleksey Lomakin for helpful discussions. FTIR and Raman measurements were carried out at the MRSEC Shared Facilities at M.I.T. supported by the National Science Foundation under award DMR-0213282 and laser facility Grant CHE-0111370. For the FTIR and Raman measurements, the generous technical assistance of Mr. Tim McClure is gratefully acknowledged.

REFERENCES

1. Aarts, H. J., den Dunnen, J. T., Leunissen, J., Lubsen, N. H., and Schoenmakers, J. G. (1988) The γ-crystallin gene families: Sequence and evolutionary patterns, *J. Mol. Evol. 27*, 163−172.
2. Hejtmancik, J. F. (1998) The genetics of cataract: Our vision becomes clearer, *Am. J. Hum. Genet. 62*, 520−525.
3. Santhiya, S. T., Shyam Manohar, M., Rawlley, D., Vijayalakshmi, P., Namperumalsamy, P., Gopinath, P. M., Loster, J., and Graw, J. (2002) Novel mutations in the γ-crystallin genes cause autosomal dominant congenital cataracts, *J. Med. Genet. 39*, 352−358.
4. Mackay, D. S., Andley, U. P., and Shiels, A. (2004) A missense mutation in the γD crystallin gene (crygd) associated with autosomal dominant "coral-like" cataract linked to chromosome 2q, *Mol. Vis. 10*, 155−162.
5. Nandrot, E., Slingsby, C., Basak, A., Cherif-Chefchaouni, M., Benazzouz, B., Hajaji, Y., Boutayeb, S., Gribouval, O., Arbogast, L., Berraho, A., Abitbol, M., and Hilal, L. (2003) γ-D crystallin gene (crygd) mutation causes autosomal dominant congenital cerulean cataracts, *J. Med. Genet. 40*, 262−267.
6. Shentu, X., Yao, K., Xu, W., Zheng, S., Hu, S., and Gong, X. (2004) Special fasciculiform cataract caused by a mutation in the γD-crystallin gene, *Mol. Vis. 10*, 233−239.
7. Burdon, K. P., Wirth, M. G., Mackey, D. A., Russell-Eggitt, I. M., Craig, J. E., Elder, J. E., Dickinson, J. L., and Sale, M. M. (2004) Investigation of crystallin genes in familial cataract, and report of two disease associated mutations, *Br. J. Ophthalmol. 88*, 79−83.
8. Pande, A., Pande, J., Asherie, N., Lomakin, A., Ogun, O., King, J. A., Lubsen, N. H., Walton, D., and Benedek, G. B. (2000) Molecular basis of a progressive juvenile-onset hereditary cataract, *Proc. Natl. Acad. Sci. U.S.A. 97*, 1993−1998.
9. Pande, A., Pande, J., Asherie, N., Lomakin, A., Ogun, O., King, J., and Benedek, G. B. (2001) Crystal cataracts: Human genetic cataract caused by protein crystallization, *Proc. Natl. Acad. Sci. U.S.A. 98*, 6116−6120.
10. Stephan, D. A., Gillanders, E., Vanderveen, D., Freas-Lutz, D., Wistow, G., Baxevanis, A. D., Robbins, C. M., VanAuken, A., Quesenberry, M. I., Bailey-Wilson, J., Juo, S. H., Trent, J. M., Smith, L., and Brownstein, M. J. (1999) Progressive juvenile-onset punctate cataracts caused by mutation of the γD-crystallin gene, *Proc. Natl. Acad. Sci. U.S.A. 96*, 1008−1012.
11. Kmoch, S., Brynda, J., Asfaw, B., Bezouska, K., Novak, P., Rezacova, P., Ondrova, L., Filipec, M., Sedlacek, J., and Elleder, M. (2000) Link between a novel human γD-crystallin allele and a unique cataract phenotype explained by protein crystallography, *Hum. Mol. Genet. 9*, 1779−1786.
12. Heon, E., Priston, M., Schorderet, D. F., Billingsley, G. D., Girard, P. O., Lubsen, N., and Munier, F. L. (1999) The γ-crystallins and human cataracts: A puzzle made clearer, *Am. J. Hum. Genet. 65*, 1261−1267.
13. Heon, E., and Munier, F. L. (2003) Personal communication.
14. Andley, U. P., Mathur, S., Griest, T. A., and Petrash, J. M. (1996) Cloning, expression, and chaperone-like activity of human αA-crystallin, *J. Biol. Chem. 271*, 31973−31980.
15. Asherie, N., Pande, J., Lomakin, A., Ogun, O., Hanson, S. R., Smith, J. B., and Benedek, G. B. (1998) Oligomerization and phase separation in globular protein solutions, *Biophys. Chem. 75*, 213−227.
16. Pande, J., Hanlon, E., and Pande, A. (2002) A comparison of the environment of thiol groups in bovine and human γ crystallins using Raman spectroscopy, *Exp. Eye Res. 75*, 359−363.
17. Broide, M. L., Berland, C. R., Pande, J., Ogun, O. O., and Benedek, G. B. (1991) Binary-liquid-phase separation of lens protein solutions, *Proc. Natl. Acad. Sci. U.S.A. 88*, 5660−5664.
18. Liu, C., Pande, J., Lomakin, A., Ogun, O., and Benedek, G. B. (1998) Aggregation in aqueous solutions of bovine lens γ-crystallins: Special role of γ(s), *Invest. Ophthalmol. Vis. Sci. 39*, 1609−1619.
19. Berland, C. R., Thurston, G. M., Kondo, M., Broide, M. L., Pande, J., Ogun, O., and Benedek, G. B. (1992) Solid−liquid-phase boundaries of lens protein solutions, *Proc. Natl. Acad. Sci. U.S.A. 89*, 1214−1218.
20. Asherie, N., Pande, J., Pande, A., Zarutskie, J. A., Lomakin, J., Lomakin, A., Ogun, O., Stern, L. J., King, J., and Benedek, G. B. (2001) Enhanced crystallization of the Cys18 to Ser mutant of bovine γB crystallin, *J. Mol. Biol. 314*, 663−669.
21. Eaton, W. A., and Hofrichter, J. (1990) Sickle cell hemoglobin polymerization, *Adv. Protein Chem. 40*, 63−279.
22. Gill, S. J., Nichols, N. F., and Wadso, I. (1976) Calorimetric determination of enthalpies of solution of slightly soluble liquids. II. Enthalpy of solution of some hydrocarbons in water and their use in establishing the temperature dependence of their solubilities, *J. Chem. Thermodyn. 8*, 445−452.
23. Gill, S. J., and Wadso, I. (1976) An equation of state describing hydrophobic interactions, *Proc. Natl. Acad. Sci. U.S.A. 73*, 2955−2958.
24. Tanford, C. (1980) *The Hydrophobic Effect: Formation of Micelles and Biological Membranes*, 2nd ed., Wiley, New York.
25. Halverson, K., Fraser, P. E., Kirschner, D. A., and Lansbury, P. T., Jr. (1990) Molecular determinants of amyloid deposition in Alzheimer's disease: Conformational studies of synthetic β-protein fragments, *Biochemistry 29*, 2639−2644.
26. Laurine, E., Gregoire, C., Fandrich, M., Engemann, S., Marchal, S., Thion, L., Mohr, M., Monsarrat, B., Michel, B., Dobson, C. M., Wanker, E., Erard, M., and Verdier, J. M. (2003) Lithostathine quadruple-helical filaments form proteinase K-resistant deposits in Creutzfeldt−Jakob disease, *J. Biol. Chem. 278*, 51770−51778.
27. Cai, S., and Singh, B. R. (2004) A distinct utility of the amide III infrared band for secondary structure estimation of aqueous protein solutions using partial least-squares methods, *Biochemistry 43*, 2541−2549.
28. Parker, F. S. (1983) Applications of infrared, Raman, and resonance Raman spectroscopy in *Biochemistry*, Plenum, New York.
29. Frushour, B. G., and Koenig, J. L. (1975) in *Advances in Infrared and Raman Spectroscopy* (Clark, R. J. H., and Hester, R. E., Eds.) pp 35−97, Heydon and Son, London, U.K.
30. Krimm, S., and Bandekar, J. (1986) Vibrational spectroscopy and conformation of peptides, polypeptides, and proteins, *Adv. Protein Chem. 38*, 181−364.
31. Bousset, L., Thomson, N. H., Radford, S. E., and Melki, R. (2002) The yeast prion ure2p retains its native α-helical conformation upon assembly into protein fibrils *in vitro*, *EMBO J. 21*, 2903−2911.
32. Steward, R. E., MacArthur, M. W., Laskowski, R. A., and Thornton, J. M. (2003) Molecular basis of inherited diseases: A structural perspective, *Trends Genet. 19*, 505−513.
33. Polymeropoulos, M. H., Lavedan, C., Leroy, E., Ide, S. E., Dehejia, A., Dutra, A., Pike, B., Root, H., Rubenstein, J., Boyer, R., Stenroos, E. S., Chandrasekharappa, S., Athanassiadou, A., Papapetropoulos, T., Johnson, W. G., Lazzarini, A. M., Duvoisin, R. C., Di Iorio, G., Golbe, L. I., and Nussbaum, R. L. (1997) Mutation in the α-synuclein gene identified in families with Parkinson's disease, *Science 276*, 2045−2047.
34. Basak, A., Bateman, O., Slingsby, C., Pande, A., Asherie, N., Ogun, O., Benedek, G. B., and Pande, J. (2003) High-resolution X-ray crystal structures of human γD-crystallin (1.25 Å) and the R58H mutant (1.15 Å) associated with aculeiform cataract, *J. Mol. Biol. 328*, 1137−1147.
35. Richardson, J. S., and Richardson, D. C. (2002) Natural β-sheet proteins use negative design to avoid edge-to-edge aggregation, *Proc. Natl. Acad. Sci. U.S.A. 99*, 2754−2759.
36. Wang, W., and Hecht, M. H. (2002) Rationally designed mutations convert de novo amyloid-like fibrils into monomeric β-sheet proteins, *Proc. Natl. Acad. Sci. U.S.A. 99*, 2760−2765.

37. Thirumalai, D., Klimov, D. K., and Dima, R. I. (2003) Emerging ideas on the molecular basis of protein and peptide aggregation, *Curr. Opin. Struct. Biol. 13*, 146−159.
38. Lo Conte, L., Chothia, C., and Janin, J. (1999) The atomic structure of protein−protein recognition sites, *J. Mol. Biol. 285*, 2177−2198.
39. Dasgupta, S., Iyer, G. H., Bryant, S. H., Lawrence, C. E., and Bell, J. A. (1997) Extent and nature of contacts between protein molecules in crystal lattices and between subunits of protein oligomers, *Proteins 28*, 494−514.
40. Czepas, J., Devedjiev, Y., Krowarsch, D., Derewenda, U., Otlewski, J., and Derewenda, Z. S. (2004) The impact of Lys → Arg surface mutations on the crystallization of the globular domain of RhoGDI, *Acta Crystallogr., Sect. D 60*, 275−280.
41. Iyer, G. H., Dasgupta, S., and Bell, J. A. (2000) Ionic strength and intermolecular contacts in protein crystals, *J. Cryst. Growth 217*, 429−440.
42. Lomakin, A., Asherie, N., and Benedek, G. B. (1996) Monte Carlo study of phase separation in aqueous protein solutions. *J. Chem. Phys. 104*, 1646−1656.
43. Lomakin, A., Asherie, N., and Benedek, G. B. (1999) Aeolotopic interactions of globular proteins, *Proc. Natl. Acad. Sci. U.S.A. 96*, 9465−9468.
44. Evans, P., Wyatt, K., Wistow, G. J., Bateman, O. A., Wallace, B. A., and Slingsby, C. (2004) The P23T cataract mutation causes loss of solubility of folded γD-crystallin, *J. Mol. Biol. 343*, 435−444.

BI0479611